Fire Safety Journal 162 (2026) 104767

Contents lists available at ScienceDirect

Fire Safety Journal

journal homepage: www.elsevier.com/locate/firesaf

A comparison of photoacoustic and grayscale measurements of soot deposition on surfaces

Amy E. Mensch *, Ryan Falkenstein-Smith, Shine Park

National Institute of Standards and Technology, 100 Bureau Drive, Gaithersburg, 20899, MD, USA

ARTICLE INFO

Keywords:
Photoacoustic
Grayscale
Soot deposition
Fire forensics

ABSTRACT

This study investigates the effectiveness of non-invasive soot deposition measurement techniques as a practical tool for fire investigators to quantify burn patterns in a fire scene. A novel technique relying on the photoacoustic effect of soot is compared to an established grayscale method. Soot was deposited on gypsum wallboard (drywall) and metal substrates mounted 97 cm, 128 cm, and 158 cm above a 13 kW propene diffusion flame burner, and the mass deposited was measured gravimetrically. Digital photographs were taken of the soot-coated substrates next to an optical density calibration target. The image grayscale values for the substrate were converted to optical density. Then the substrates were perturbed with a camera flash, and the photoacoustic response of the soot was measured by a microphone as the peak sound pressure. The best-fit curve for the optical density data versus soot mass loading was linear, while the photoacoustic response and was log-based, with the photoacoustic method producing a higher correlation coefficient. The photoacoustic correlation was dependent on the flash intensity, with similar photoacoustic responses for both drywall and metal substrates.

1. Introduction

In forensic fire reconstruction, investigators attempt to draw conclusions about fire origin, the direction of fire progression, and the duration of fire exposure by relying on the subjective interpretation of post-fire burn patterns. This analysis involves characterizing the soot that forms burn patterns on surfaces and linking soot deposition to critical elements of the fire. In fire research, soot deposition measurements are also important for validating life-safety predictions from fire models, such as the National Institute of Standards and Technology (NIST)'s Fire Dynamics Simulator (FDS) [1]. In FDS, soot deposition mechanisms represent a sink in the carbon mass balance and thus affect smoke concentration, enabling FDS to predict occupant exposures such as smoke visibility and toxicity.

The driving mechanisms of soot deposition are understood to be thermal gradients near surfaces (thermophoresis), turbulence, and gravity. However, the ability to accurately predict soot deposition in fires has been limited by difficulties in measuring both the fire conditions and the soot deposition itself.

In a research setting, point measurements of deposition can be made using gravimetric targets [2,3] or conductometric gauges [4,5]. These established methods can provide high accuracy (gravimetric) or time-resolution (conductance) but require modification of the substrate prior to exposure, rendering them unsuitable for fire investigations. A possible post-fire soot measurement method relying on grayscale image analysis was demonstrated by Riahi [6,7]. The non-invasive technique involved placing white glass paper filters on a wall next to fires from burning gasoline or polymer materials. After collecting soot on the filters, Riahi imaged the filters alongside a standard grayscale target using a flatbed scanner to assign the target's optical density values. The mass of the filters was also measured before and after soot exposure to obtain gravimetric measurements of the deposited soot, ranging from 300 mg/m^2 to 400 mg/m^2, and compared to the optical densities. Riahi then applied the method to the full wall by imaging it with a digital camera, yielding local optical density contour maps that could be converted to soot mass distributions using the relationship from the filter tests. Since digital photography of soot deposition patterns is readily available in the field, the grayscale technique requires only an additional optical density target. However, the effects of inconsistent lighting or different substrates (other than an opaque, white surface) on the grayscale technique have not been investigated. Also, higher amounts of deposition may not be distinguishable from each other since the grayscale value may not change for surfaces that are already coated.

Photoacoustic properties of soot have previously been leveraged to measure the aerosol concentration of soot and soot emissions [8–11]. Due to soot's absorptive properties, particulates are rapidly heated

* Corresponding author.
E-mail address: amy.mensch@nist.gov (A.E. Mensch).

https://doi.org/10.1016/j.firesaf.2026.104767
Received 24 April 2025; Received in revised form 7 February 2026; Accepted 23 March 2026
Available online 25 March 2026
0379-7112/Published by Elsevier Ltd.

Fig. 1. Photo of the burner and substrate setup for soot deposition.

when exposed to modulated light, creating a subsequent thermal expansion of the surrounding gas which produces a sound wave. Refs. [8,9] demonstrated that the intensity of the generated acoustic signal is proportional to the absorbed energy, thus establishing a method to measure soot mass concentration in a gas.

There have been several works that have used this effect to develop tools for practical applications. Beck et al. [10] characterized a mobile photoacoustic soot aerosol sensor designed for diesel engine exhaust with a detection limit of 2.0 $\mu g/m^3$ and a temporal resolution of approximately 1 s. Humphries et al. examined this photoacoustic effect within a flame using a high-power laser and a MEMS microphone at the burner surface, of which the results successfully identified the onset of soot formation at specific heights within the flame envelope.

Although previously developed techniques demonstrate value in measuring soot aerosol suspended in a gas, they do not apply to quantifying soot deposition on a surface. The current study investigates the feasibility of implementing a photoacoustic measurement technique for post-fire soot deposition. The results from the photoacoustic and grayscale techniques are directly compared under reproducible conditions of soot deposition on two types of substrates.

2. Methods

Soot was deposited on substrates typically found in buildings, such as gypsum wallboard (referred to in this work as drywall) and stainless steel (referred to in this work as metal) surfaces using a 13 kW propene fire in a 10 cm diameter, 13.3 cm high, uncooled burner for a 30 min exposure time, as shown in Fig. 1. The burner was filled with spherical copper beads approximately 3.1 mm in diameter, up to 1 cm below the top of the burner. The 30 cm × 46 cm substrates were mounted directly above the burner at different heights from the burner surface to deposit different amounts of soot. The drywall substrates were 1.27 cm thick and mounted at 97 cm, 128 cm, and 158 cm above the burner surface. The stainless steel substrates were 0.07 cm thick and collected soot at 97 cm and 158 cm from the burner surface. In all cases, the substrate was mounted well above the visible flame of the fire.

Fig. 2. Example grayscale image of the density step target next to a drywall substrate coated with soot 128 cm from the burner, also showing the circular region of interest on the substrate.

After soot was deposited, the substrate was mounted vertically on an aluminum frame, and three to four digital images were taken of each substrate next to an Edmund Optics Density Step Target[1] in the same frame, as shown in Fig. 2 for a drywall substrate at 128 cm from the burner. The camera used in this work was a Casio EX-100F, which captured images at an F-stop of f/2.8, an exposure time of 1/60 s, and an ISO speed range of ISO-125 to ISO-160. The images were converted to grayscale values, GS, ranging from 0 (black) to 255 (white) at each pixel. The images were in 8-bit JPEG format, which limits the grayscale resolution to 256 intensity levels, but this compact and practical image format is more likely to be used in the field compared to RAW images.

A circular region of interest encompassing the substrate's center was used to compute the average GS for each substrate image. The ROI contained about 160k pixels on average, and the standard deviation across the pixels was about 10% of the average GS. Then these area-averaged GS values were averaged across the three to four images of each substrate. The circular region of interest, shown in Fig. 2, has a radius of 5.9 cm, which is the area where targets were placed to measure the mass of soot deposition, as described later.

The density step target was used to generate a calibration curve to convert the average GS for each substrate to OD. The density step target contained 15 steps, each assigned an optical density value, OD, from 0.1 (lightest) to 1.5 (darkest), with increments of 0.1. The average GS at each target step was plotted against the corresponding OD. A

[1] Certain commercial equipment, instruments, or materials are identified in this paper in order to specify the procedures adequately. Such identification is not intended to imply recommendation or endorsement by the National Institute of Standards and Technology, nor is it intended to imply that the materials or equipment identified are necessarily the best available for the purpose.

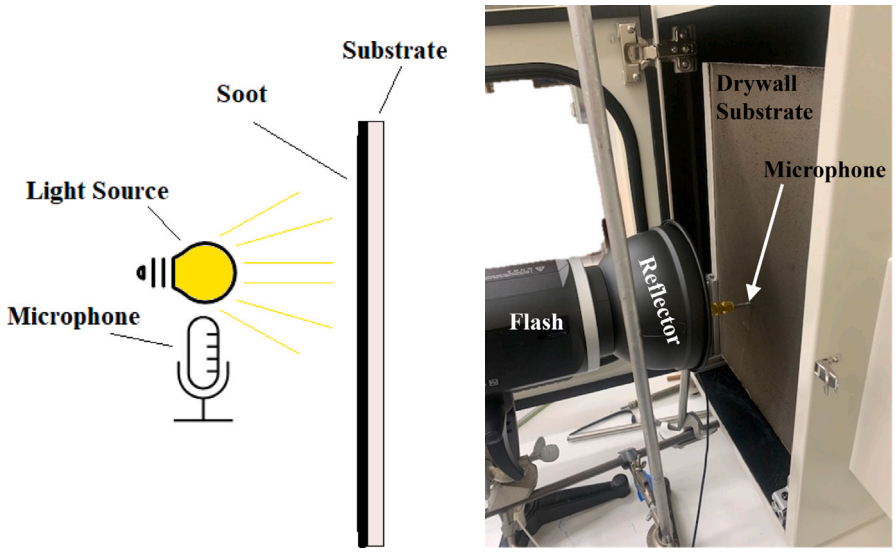

Fig. 3. Photoacoustic measurement setup, showing (a) a schematic of the key components and (b) a photo of the substrate in the sound isolation chamber with the flash, reflector, and microphone in place.

curve fit was made between the OD and GS data in the form of a Rodbard function, given in Eq. (1), with fit constants a, b, c, and d.

$$OD = \frac{a-d}{1+(\frac{GS}{c})^b} + d \tag{1}$$

Next, the substrate on the aluminum frame was placed just inside the opening of a sound-isolation chamber, in front of the photoacoustic measurement setup shown in Fig. 3, to measure the soot's photoacoustic response. The light source was generated from a commercial LED camera flash (Flashpoint, FPLFX600B) with a cone-shaped reflector to focus the light. The reflector, with a radius of 9 cm, was pointed at the center of the substrate 7.0 cm away from the surface. At this location, the flash illuminates a circular area with a radius of approximately 14 cm on the substrate. Two flash settings were used to produce different light intensities. The settings were expressed in the amount of optical output energy delivered from the time of the flash firing until the energy decayed to 10% of the peak. The settings were 600 J in 0.0045 s and 2.3 J in 0.0001 s for the drywall substrate. When later collecting data for the metal substrate, the focus was on the higher flash intensity, which generated a stronger acoustic response. The acoustic measurements were recorded with a high-sensitivity microphone (GRAS Acoustics, 46BE) able to measure up to 2325 Pa. The microphone signal was recorded at a rate of 48 kHz, and converted from voltage to sound pressure using the calibration factor provided by the manufacturer, 0.2258 Pa/mV. The microphone was positioned between the flash and the substrate, approximately 0.5 cm from the substrate. This setup, as shown in Fig. 1b, maintained the orientation of the microphone and enabled measurement of an acoustic signal distinguishable from the baseline. The sound pressure over time was recorded for three repeated flashes, and the peak sound pressures were averaged. The average peak from a blank substrate without any soot is subtracted to compute the photoacoustic response.

The amount of soot deposited on the substrate at each condition was measured using gravimetric targets, similar to those used in Mensch and Cleary [3]. A second substrate was prepared for each condition with five pre-weighed aluminum foil targets, 0.03 mm thick, on the substrate. The targets were taped to the substrate to expose a square area of 2.52 cm^2 to the soot deposition. One target was taped in the center of the substrate, and the other four were on each side of the center target with a 5.1 cm distance between the center of the targets. The five targets were within the circular region of interest outlined in Fig. 2. After the soot was deposited, the tape was removed with tweezers, and the change in mass of the target over the target area provided the soot load. The five soot load measurements on each substrate were averaged together to compare with the grayscale measurements and the photoacoustic response for each substrate condition.

3. Results

The gravimetric soot deposition mass load measurements are plotted in Fig. 4 for all targets as a function of the substrate height above the burner. The average soot mass load at each distance is reported in Table 1 along with the 95% expanded uncertainty based on the standard deviations between gravimetric targets. There was no consistent trend in the target masses based on target location. The mass load for the 158 cm height is an average across targets from two repeat substrates. The difference between the averages for the repeat substrates is 10 mg/m^2 (8.8%). Additionally, soot deposition mass loads were measured on larger 61 cm × 61 cm drywall substrates 158 cm from the same burner in this study, with the setup described in [12,13]. The average soot mass load for gravimetric targets at a 3.75 cm radius was 110 mg/m^2, which is within the uncertainty reported in Table 1 for the targets within a 5.1 cm radius in this study. Overall, considering the mass loads measured from both substrate sizes at 158 cm, five repeat experiments showed agreement in the mass loads measured, confirming reproducibility of the deposition process.

While the deposition dependencies on substrate type or height above the burner are not the focus of this paper, the authors observed a few trends that affect the soot mass loads used to evaluate the photoacoustic and grayscale methods. Soot deposition decreases as the burner is moved away from the substrate for the 30 min exposure. There is more scatter in the target measurements when the substrate is closest to the burner, at 97 cm, compared to the targets at the other two heights. This is likely due to spatial variation in the deposition at 97 cm, while the plume has more opportunity to mix and spread when the substrate is farther away. Compared with drywall, more soot deposition is observed on the metal substrate at 97 cm, but little difference between the substrates at 158 cm. The reason for these

Table 1
Average mass load of soot as measured by gravimetric targets.

Substrate	Distance from burner (cm)	Mass Load[a] (mg/m^2)
Drywall	97	597 ± 149
	128	273 ± 29
	158	114 ± 17
Metal	97	875 ± 170
	158	95 ± 35

[a] ± 95% expanded uncertainty

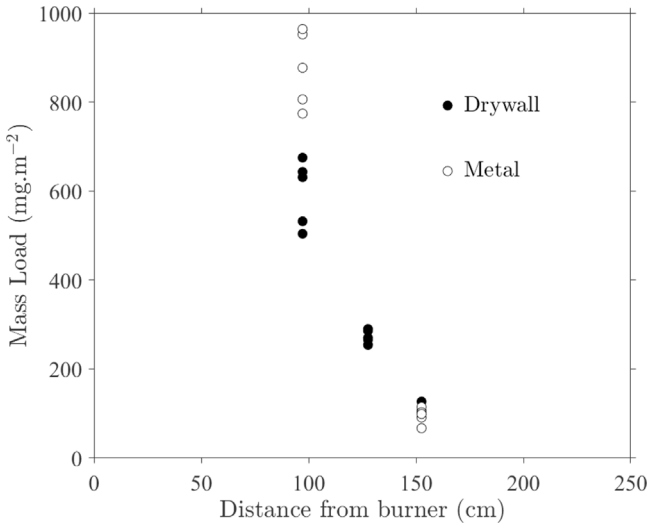

Fig. 4. Gravimetric measurements of soot mass load after a 30 min exposure as a function of substrate height above the burner.

differences is the metal substrate's better heat dissipation, resulting in a cooler surface temperature on the deposition surface. The difference occurs because the substrates are closer to the burner due to greater heat transfer from the fire.

3.1. Grayscale measurements

The Rodbard calibration function used to convert the image *GS* to *OD* is shown in Fig. 5. This correlation was obtained from the image of the density step target with the highest R^2 correlation coefficient and used to convert the average *GS* for each substrate to *OD*. The average *GS* for each substrate was the average value across the substrate region of interest (as shown in Fig. 2) among the three or four repeat images of the same substrate.

The average *OD* of each substrate is plotted in Fig. 6 as a function of the average soot mass load measured for that experimental condition. Drywall results are presented as circles, and metal results are presented as triangles. Multiple data points plotted for the same mass load correspond to the *OD* from distinct substrates exposed to the same soot deposition conditions. The vertical error bars in *OD* represent the 95% expanded uncertainty arising from repeat images of the same substrate, although repeat images were taken in the same location and configuration. The horizontal error bars show the 95% expanded uncertainty based on the standard deviations between the mass load measurements taken for each substrate condition.

All *OD* data points appear to increase similarly with mass load except for the metal substrate around 900 mg/m^2, which measured about the same or lower *OD* as the drywall substrates with around 600 mg/m^2. Excluding this point, a linear fit line has the highest correlation coefficient (R^2 = 0.89). A linear correlation between the *OD* and soot mass loads of up to 300 mg/m^2 was reported by Riahi [6]. The leveling off of *OD*, around 1 to 1.5 for mass loads above 600 mg/m^2,

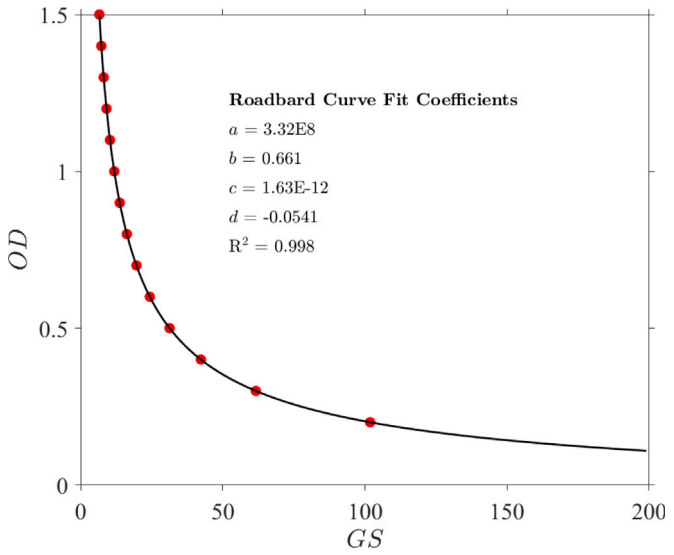

Fig. 5. Correlation between *OD* and image *GS* for the density step target, including the coefficients for the Rodbard function curve fit, given in Eq. (1).

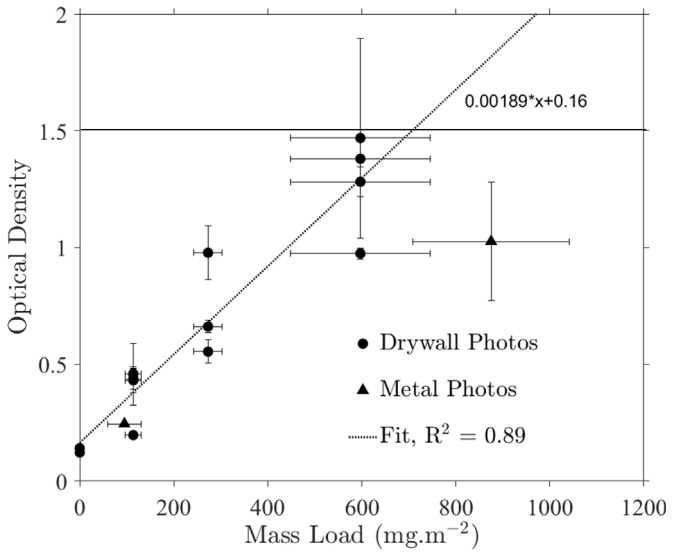

Fig. 6. Correlation of the average *OD* of each substrate to the average mass loading for that case. A line at *OD* = 1.5 indicates the maximum value on the *OD* target. Error bars show the 95% expanded uncertainty of the average measurement for each substrate.

despite increasing soot mass load, is expected since 1.5 is the maximum value for the optical density target (indicated by a horizontal line). At low *GS* values, the *OD* is very sensitive to small changes in *GS* (Fig. 5), hence the large *OD* uncertainty for some data points above 600 mg/m^2. This indicates it is difficult to detect differences in soot mass load above 600 mg/m^2 using the grayscale method. The metal substrates also appear to generate lower *OD* values than expected based on their measured soot mass load and the overall trend line.

3.2. Photoacoustic measurements

The raw photoacoustic response of soot deposition on drywall is shown in Fig. 7. Fig. 7(a) shows the response to a single flash for four different mass load cases at the 600 J flash setting. For the cases with non-zero soot deposition, the measured signal is initiated with a sharp positive peak, which then drops to negative value and slowly

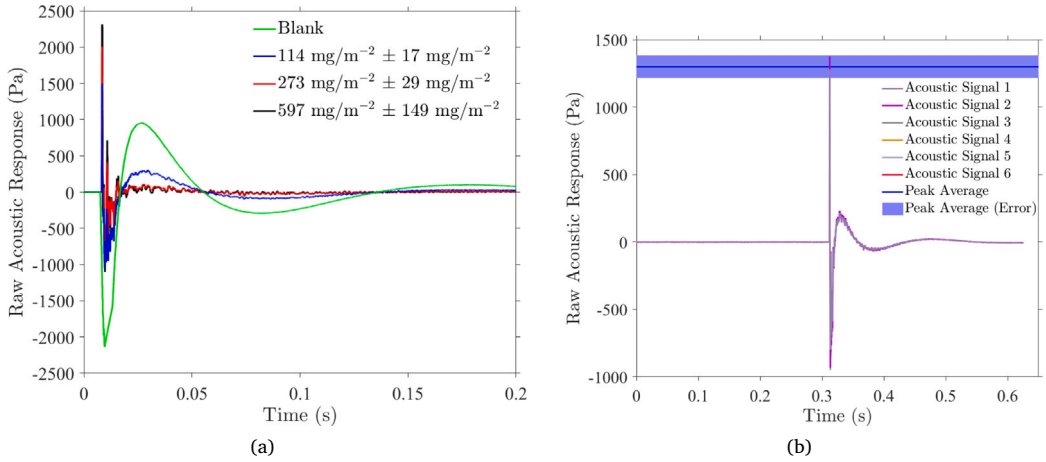

Fig. 7. Measurements of the raw acoustic response of soot deposited on drywall with the 600 J light setting, showing (a) a single flash for four different mass load cases at the 600 J flash setting and (b) repeated measurements on a board with 114 mg/m^2 along with the average peak value and associated error (95% confidence).

oscillates until reaching the baseline. Therefore, the magnitude of the initial positive peak is assumed to be representative of the acoustic response from the soot. The initial positive peaks have all been aligned so it can be seen that their magnitude increases with soot mass load. For the blank substrate without any soot, there is still a measured sound pressure, but the response instead begins with an initial negative peak, which occurs after the positive peaks from soot-coated substrates. Because of the distinct differences in the measured sound pressure with a blank substrate, this response is likely a result of the sound coming from the flash shutter.

Repeated measurements of the raw acoustic response of soot deposition are shown in Fig. 7(b) for a drywall board with 114 mg/m^2 soot mass load. These measurements are taken for flashes a few seconds apart at the 600 J light setting, and the average peak and associated standard uncertainty (95% confidence) are shown in blue. Fig. 7(b) demonstrates the repeatability of the sound pressure measurement because there is no trend in the raw acoustic response with repeated exposures. Therefore, to determine the photoacoustic response for each substrate, three successive positive peak responses are averaged together.

The photoacoustic response of each substrate is plotted in Fig. 8 as a function of the average soot mass load measured for that experimental condition. Drywall results are presented as circles or squares, and metal results are presented as triangles. Filled symbols show the responses from the higher intensity flash, 600 J, and open symbols show the responses from the lower intensity flash, 2.3 J. Repeated drywall cases with the high-intensity flash show good agreement. The error bars show the 95% expanded uncertainty of the average acoustic response and the average mass load measurements for each substrate. The acoustic responses for the high-intensity flash and the highest mass load cases (above 600 mg/m^2) are very close to the maximum range of the microphone, 2325 Pa. The similar values are due to microphone limitations, which could be addressed by adjusting the microphone distance or reducing the light intensity, as the low-intensity flash results do not approach the limit.

Looking at the rest of the high-intensity flash results and the low-intensity flash results, the slope of the photoacoustic response begins to reduce or level off as the mass load increases. Therefore, log-based fits were used to correlate acoustic responses with mass load regardless of substrate material. As expected, the acoustic response is lower and levels off sooner for a lower flash intensity. Although data for lower flash intensity was collected only for the drywall substrate, it is

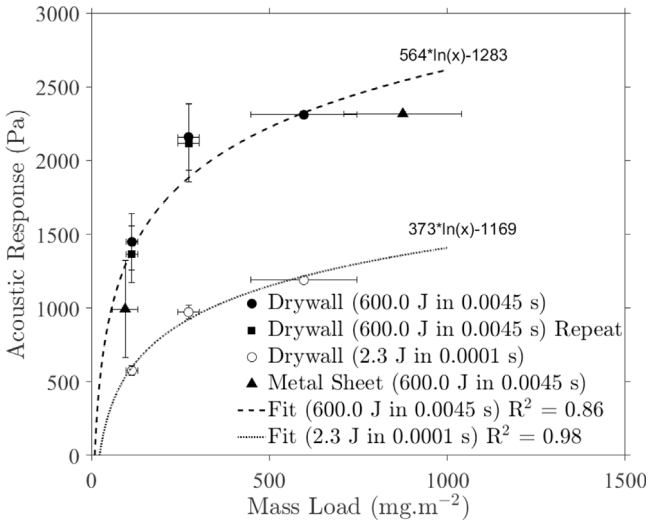

Fig. 8. Correlation of the average acoustic response to the average mass loading for each substrate case. Different curve fits are drawn for the two different flash settings. Error bars show the 95% expanded uncertainty of the average measurement for each substrate.

assumed that the same trend of lower response at lower flash intensity would apply to other substrate materials. Two different log-based curve fits are plotted for the two flash intensities, which intersect the error bars of most of the data points and have R^2 values of 0.86 for the high-intensity flash and 0.98 for the low-intensity flash. The combined data from both substrates produce a fairly high correlation coefficient for the high-intensity flash. In comparison, the correlation from the low-intensity flash is even better since the lower acoustic responses are not limited by the microphone range.

The logarithmic relationship between the acoustic response and the mass load means that the uncertainty in the mass load determined by this method changes depending on the amount of soot. The mass load resolution is high at light mass loads, but the resolution decreases as the mass increases. It is not surprising that the response begins to level off as the mass load increases, because as the thickness of the soot

layer grows, it may become more difficult to expose all of the soot to the flash. This effect could limit the photoacoustic response that can be measured if the mass load increases further, even when the sound pressure is within the microphone's range. The lower limit of detection for the photoacoustic technique has not been determined, but the high intensity log fit predicts a measurable acoustic response above 10 mg/m^2.

Fig. 8 also demonstrates that the photoacoustic response is similar for both drywall and metal substrates, which is important for the practicality of using photoacoustic measurement tools in real applications. Using the correlations in Fig. 8, measurements of the photoacoustic response with the same flash and microphone setup can be used to quantify the soot mass load on different types of surfaces. Comparing the grayscale and photoacoustic measurements from this study, the photoacoustic method generates similar or higher correlation coefficients with the measured soot mass loads compared to the grayscale method.

4. Conclusions

This study explored the measurements from two non-invasive and practical techniques to compare their correlations with soot deposition on surfaces. The grayscale technique showed a reasonable correlation between the image's optical density and the actual soot mass load. The grayscale technique was limited by the finite range of the optical density target, as evidenced by significant uncertainty and a lack of a clear increase in optical density at mass loads of 600 mg/m^2 and higher.

The photoacoustic technique measured the acoustic response of deposited soot to a flash of light, which was plotted against gravimetric measurements to give a log-based correlation based solely on the flash intensity. The photoacoustic correlations yielded similar or higher correlation coefficients than the grayscale correlation, demonstrating the reproducibility of the photoacoustic measurements. The results showed that the acoustic response was consistent between the two substrates and was based only on the mass load and flash intensity.

Tools for quantifying soot deposition could be particularly useful for fire forensic investigations that rely on burn patterns. Traditional methods for characterizing soot deposition are either qualitative or applicable only in a research setting. The current study demonstrated the potential of photoacoustic measurements to provide a better understanding of soot deposition and burn patterns, both in fire research and fire investigations. Before its application in the field, future development of the photoacoustic technique should focus on optimizing the setup and understanding limitations that may exist outside of a controlled laboratory setting. This includes determining the limits of detection of the method and evaluating the photoacoustic response in more realistic environments, such as full-scale or field experiments.

CRediT authorship contribution statement

Amy E. Mensch: Writing – original draft, Visualization, Methodology, Formal analysis, Data curation, Conceptualization. **Ryan Falkenstein-Smith:** Writing – review & editing, Visualization, Methodology, Formal analysis, Data curation, Conceptualization. **Shine Park:** Visualization, Formal analysis.

Declaration of competing interest

The authors declare that they have no known competing financial interests or personal relationships that could have appeared to influence the work reported in this paper.

Acknowledgments

The authors acknowledge the input from NIST colleagues, Thomas Cleary, Marco Fernandez, and Michael Selepak, as well as funding from NIST's Engineering Laboratory.

Data availability

Data will be made available on request.

References

[1] K. McGrattan, R. McDermott, M. Vanella, E. Mueller, S. Hostikka, J. Floyd, Fire dynamics simulator user's guide 6th edition, Tech. Rep. NIST SP 1019, National Institute of Standards and Technology, Gaithersburg, MD, 2024, http://dx.doi.org/10.6028/NIST.SP.1019.

[2] S. Riahi, C.L. Beyler, J. Hartman, Wall smoke deposition from a hot smoke layer, Fire Technol. 49 (2) (2013) 395–409, http://dx.doi.org/10.1007/s10694-012-0273-x, URL http://link.springer.com/10.1007/s10694-012-0273-x.

[3] A.E. Mensch, T.G. Cleary, Measurements and predictions of thermophoretic soot deposition, Int. J. Heat Mass Transfer 143 (2019) 118444, http://dx.doi.org/10.1016/j.ijheatmasstransfer.2019.118444.

[4] A. Mensch, T. Cleary, A soot deposition gauge for fire measurements, NIST Technical Note 1985, National Institute of Standards and Technology, 2018, URL https://doi.org/10.6028/NIST.TN.1985.

[5] A. Reynaud, M. Leblanc, S. Zinola, P. Breuil, J.-P. Viricelle, Responses of a resistive soot sensor to different mono-disperse soot aerosols, Sensors 19 (3) (2019) http://dx.doi.org/10.3390/s19030705.

[6] S. Riahi, Development of Tools for Smoke Residue and Deposition Analysis (Ph.D. thesis), George Washington University, 2010.

[7] S. Riahi, C. Beyler, Measurement and prediction of smoke deposition from a fire against a wall, Fire Saf. Sci. 10 (2011) 641–654, http://dx.doi.org/10.3801/IAFSS.FSS.10-641.

[8] A. Petzold, R. Niessner, Photoacoustic sensor for carbon aerosols, Sensors Actuators B: Chem. 14 (1–3) (1993) 640–641, http://dx.doi.org/10.1016/0925-4005(93)85126-U.

[9] C. Haisch, R. Niessner, Light and sound—photoacoustic spectroscopy, Spectrosc. Eur. (2002).

[10] H.A. Beck, R. Niessner, C. Haisch, Development and characterization of a mobile photoacoustic sensor for on-line soot emission monitoring in diesel exhaust gas, Anal. Bioanal. Chem. 375 (8) (2003) 1136–1143, http://dx.doi.org/10.1007/s00216-003-1810-8.

[11] G.S. Humphries, J. Dunn, M.M. Hossain, M. Lengden, I.S. Burns, J.D. Black, A simple photoacoustic method for the in situ study of soot distribution in flames, Appl. Phys. B 119 (4) (2015) 709–715, http://dx.doi.org/10.1007/s00340-015-6132-y.

[12] E. Veley, A. Mensch, R. Falkenstein-Smith, T. Cleary, Estimations of photophoresis and thermophoresis impacts on soot particle velocity, in: Proceedings of the Spring 2024 Meeting of the Eastern States Section of the Combustion Institute, Athens, GA, 2024.

[13] E. Veley, A. Mensch, R. Falkenstein-Smith, T. Cleary, M. Vanella, J. Hodges, Effects of heat transfer models on soot deposition, in: Computational Methods for Multi-Scale, Multi-Uncertainty and Multi-Physics Problems, Porto, Portugal, 2025.